RSC Advances

PAPER

View Article Online
View Journal | View Issue

Cite this: *RSC Adv.*, 2025, **15**, 10243

Identification of acrylamide-based covalent inhibitors of SARS-CoV-2 (SCoV-2) Nsp15 using high-throughput screening and machine learning†

Teena Bajaj,‡[a] Babak Mosavati,‡[bc] Lydia H. Zhang,[d] Mohammad S. Parsa,[e] Huanchen Wang,[f] Evan M. Kerek,[g] Xueying Liang,[h] Seyed Amir Tabatabaei Dakhili,[i] Eddie Wehri,[j] Silin Guo,[k] Rushil N. Desai,[c] Lauren M. Orr,[k] Mohammad R. K. Mofrad,[l] Julia Schaletzky,[jm] John R. Ussher,[i] Xufang Deng,[h] Robin Stanley,[f] Basil P. Hubbard,[g] Daniel K. Nomura[k] and Niren Murthy*[h]

Non-structural protein 15 (Nsp15) is a SARS-CoV-2 (SCoV-2) endoribonuclease and is a promising target for drug development because of its essential role in evading the host immune system. However, developing inhibitors against Nsp15 has been challenging due to its structural complexity and large RNA binding surface. In this report, we screened a 2640 acrylamide-based compound library against Nsp15 and identified 10 fragments that reacted with cysteine residues on Nsp15 and inhibited its endoribonuclease activity with IC_{50}s less than 5 μM. These compounds had several attractive properties, such as low molecular weight (180–300 g mol^{-1}), log *P* <3, zero violations to Lipinski's rules, and no apparent pan-assay interference (PAINs) properties. In addition, based on this data as a training set, we developed an artificial intelligence (AI) model that accelerated the hit to lead process and had a 73% accuracy for predicting new acrylamide-based Nsp15 inhibitors. Collectively, these results demonstrate that acrylamide fragments have great potential for developing Nsp15 inhibitors.

Received 27th September 2024
Accepted 25th February 2025

DOI: 10.1039/d4ra06955b

rsc.li/rsc-advances

Introduction

The emergence and rapid spread of the SARS-CoV-2 (SCoV-2) virus has stimulated the need for new drugs. Hundreds of drug discovery campaigns have been run to target essential proteins from SCoV-2 virus.[1,2] For example, targeting RNA dependent RNA polymerase (RdRp)[3] and main protease (Mpro)[4,5] has led to the discovery of several promising antiviral drugs. However, alternative drugs that target other crucial proteins from SCoV-2 are still needed to respond to strain evolution and resistance development.[6,7] The non-structural protein 15 (Nsp15) is a promising therapeutic target for drug development against SCoV-2 because its inhibition results in the upregulation of interferons and protects against viral infections *via* multiple pathways.[8,9]

Nsp15 cleaves viral RNA and suppresses host sensors that recognize viral RNA and induce the production of interferons.[10] Inhibition of Nsp15 activates the production of interferons and prevents the spread of viral infection through paracrine signaling pathways, consequently the activation of Nsp15 in a few cells can have global effects on anti-immunity.[11] For example, infection of lung-derived epithelial cell lines and

[a]*Graduate Program of Comparative Biochemistry, University of California, Berkeley, Berkeley, CA, USA. E-mail: bajajtiya@berkeley.edu*
[b]*Innovative Genomics Institute, University of California, Berkeley, Berkeley, CA, USA. E-mail: bmosavati@berkeley.edu*
[c]*Department of Bioengineering, University of California, Berkeley, Berkeley, CA, USA*
[d]*Graduate Program of Molecular Toxicology, University of California, Berkeley, Berkeley, CA, USA*
[e]*Department of Applied Science and Technology, University of California, Berkeley, CA, USA*
[f]*Signal Transduction Laboratory, National Institute of Environmental Health Sciences, National Institutes of Health, Department of Health and Human Services, North Carolina, USA*
[g]*Department of Pharmacology, Li Ka Shing Institute of Virology, University of Alberta, Edmonton, Alberta, Canada*
[h]*Department of Physiological Sciences, College of Veterinary Medicine, Oklahoma Center for Respiratory and Infectious Disease, Oklahoma State University, Oklahoma, USA. E-mail: nmurthy@berkeley.edu*
[i]*Faculty of Pharmacy and Pharmaceutical Sciences, University of Alberta, Edmonton, Alberta, Canada*
[j]*The Henry Wheeler Center for Emerging and Neglected Diseases, University of California, Berkeley, Berkeley, CA, USA*
[k]*Department of Chemistry, University of California, Berkeley, Berkeley, CA, USA*
[l]*Department of Mechanical Engineering, University of California, Berkeley, CA, USA*
[m]*The Molecular Therapeutics Initiative, University of California, Berkeley, 344 Li Ka Shing, Berkeley, CA, USA*

† Electronic supplementary information (ESI) available. See DOI: https://doi.org/10.1039/d4ra06955b

‡ Equal contribution by authors.

primary nasal epithelial air–liquid interface (ALI) cultures with mutant Nsp15 SCoV-2 virus caused an increased secretion of interferons and attenuated viral replication significantly.[12] In another instance, infection of mutant Nsp15 MHV coronavirus into mouse bone marrow-derived macrophages resulted in an early and robust induction of interferon leading to rapid cell death.[8] This suggests that viruses with mutant Nsp15 cannot infect mice effectively, due to their activation of the host immune response.[8] Additionally, Nsp15 is also an evolutionarily conserved protein,[13] with a possibility of discovering inhibitors efficacious against other coronaviruses. Though Nsp15 has great potential as a drug target, it is less explored in terms of drug discovery due to the challenge of drugging its very large binding interface.[14] Only a handful of compounds have been identified that can inhibit Nsp15.[15–17]

Targeted covalent inhibition could be a promising route to drug classically "undruggable" proteins, such as Nsp15. SCoV-2 Nsp15 has several free cysteines (five cysteines: Cys103, Cys117, Cys291, Cys293 and Cys334) that play a role in subunit oligomerization and interactions with the RNA substrate that can potentially be targeted by covalent drugs. There is evidence that alkylation or other types of covalent modification of these cysteines by covalent drugs might have the potential to inhibit Nsp15 activity.[16] Irreversible covalent modification of the cysteine near the active site is likely to be implicated in the mechanism of inhibition of Nsp15 through these compounds. However, electrophile libraries of covalent inhibitors have never been investigated before for identifying Nsp15 inhibitors.

In this report, we screened an acrylamide-based electrophile library containing 2640 compounds against Nsp15 and identified several fragments that inhibited Nsp15 with IC_{50}s less than 5 μM, which had specificity for Nsp15 over other cysteine containing proteins. We selected an acrylamide library for screening because of their high selectivity for thiol nucleophiles and moderate reactivity to thiols at physiological pH. The identified fragments have promising predicted pharmacological properties and follow Lipinski's rule of five and are easy to synthesize. Mass spectrometry experiments showed that one of the ten compounds we identified modified the cysteine next to the Nsp15 active site (residue Cys293). Building on this, we used our experimental data to develop an innovative artificial intelligence platform that can predict potential inhibitors of Nsp15 and demonstrated that it has high prediction accuracy of ∼80%. Thus, this work both identifies a new chemical scaffold for the development of future drugs targeting SCoV-2 *via* Nsp15 and illustrates a novel approach to expedite the discovery and optimization of lead hits in a faster, and more economical manner. In conclusion, we demonstrate acrylamide-based Nsp15 inhibitors are interesting lead compounds for future drug discovery campaigns against coronaviruses.

Results and discussion

Rationale for selecting an acrylamide library to identify covalent inhibitors against SCoV-2 Nsp15

To discover covalent inhibitors that could sustain engagement efficiently with minimal off-target reactivity, we targeted the most nucleophilic residues present on the Nsp15 protein, those being cysteine residues.[18] Typically, the most used electrophile building block employed in covalent inhibitors targeting cysteines are Michael acceptors, such as acrylamides.[19] Acrylamides have been widely used as electrophiles in irreversible covalent inhibitors for many proteins bearing non-catalytic cysteines. For example, afatinib,[20] ibrutinib,[21] and AMG-510 (ref. 22) are acrylamide-based inhibitors of EGFR, BTK, and K-RasG12C, respectively.[23] Here, we used an electrophile library containing 2640 acrylamide compounds from Enamine.

Acrylamide-based compounds are covalent inhibitors against SCoV-2 Nsp15

Hexameric Nsp15 was recombinantly expressed and purified from bacterial cells using talon and size exclusion chromatography.[13] We utilized two parameters (binding and inhibiting Nsp15) to discover acrylamide-based covalent inhibitors from high-throughput screening (HTS) (Fig. 1A). First, we used an activity-based protein profiling (ABPP) probe, cysteine-reactive tetramethylrhodamine-5-iodoacetamide dihydroiodide (IA-Rho)[24] in a competitive manner to screen the acrylamide library to facilitate the discovery of covalent ligands against SCoV-2 Nsp15. The presence of cysteine-reactive compounds was expected to correspond with the disappearance of the IA-Rho-labeled Nsp15 band which can be visualized *via* gel electrophoresis for detection of Rho. We optimized the Nsp15 and IA-Rho concentrations to 0.25 μg and 0.5 μM, respectively. The negative control consisted of Nsp15, IA-Rho and DMSO. We initiated high throughput screening at a final concentration of 40 μM. A concentration of 40 μM was selected for the screening because Nsp15 is an undruggable target and would likely require high concentrations of compounds to identify inhibitors. We screened 2640 acrylamide-based compounds at a final concentration of 40 μM and the compounds that led to disappearance of the Nsp15 band were selected, followed by their confirmation with repurchased compounds. Repurchased compounds refer to the hits repurchased from ChemDiv as single compounds. Promising hits were repurchased to validate their activity further characterize them. The preliminary screening of the acrylamide library identified 829 initial hits that reacted with Nsp15 *via* its cysteines, corresponding to a hit rate of 31.4%.

To further characterize and validate the potential binders as Nsp15 inhibitors, we used a fluorescence-based HTS assay that uses a DNA–RNA hybrid oligomer (5′FAM-dArUdAdA-TAMRA3′) with FRET pairs on the ends.[25,26] As Nsp15 preferentially cleaves uridylates (rU),[25] the endonuclease cleavage of this substrate determines the specific cleavage by Nsp15. Endonuclease cleavage of the oligomer by Nsp15 was quantified by measuring the fluorescence after exciting at 485 nm and measuring the emission at 535 nm. The optimized concentrations, Nsp15 (5 nM) and substrate (1 μM) showed a significant difference (>5-fold) between negative (in absence of Nsp15) and positive control (in presence of Nsp15) and had a Z' calculated as >0.5. The dataset was normalized with negative and positive control and percentage inhibition was calculated.[25,26] The screening of

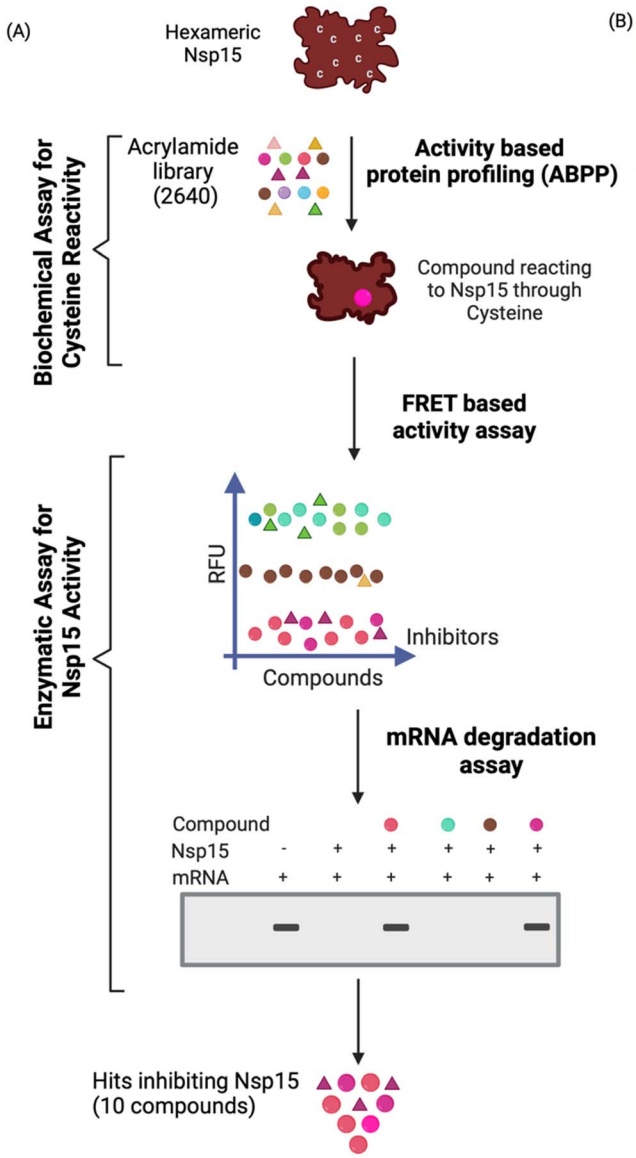

(B)

Compound	IC_{50} (μM)	Chemical Structure
1	1.50	
2	4.72	
3	1.64	
4	3.46	
5	1.11	
6	1.48	
7	3.22	
8	2.21	
9	0.99	
10	3.16	

Fig. 1 High-throughput screening (HTS) of acrylamide library consisting of 2640 compounds against Nsp15 identified ten inhibitors with sub-micromolar IC_{50}s. (A) Hexameric Nsp15 was screened against the acrylamide library using three HTS assays including activity-based protein profiling (to find cysteine binders) and FRET and mRNA degradation assay (to find inhibitors) at the concentration of 40 μM; (B) ten potent covalent inhibitors of Nsp15 that have IC_{50}s less than 5 μM were identified, and their chemical structures are shown.

initial hits using this FRET assay resulted in the identification of 408 compounds (a hit rate of 15.4%) that inhibited endonuclease activity of Nsp15. To rule out the false positives, an orthogonal assay was performed to find out if these compounds could prevent mRNA degradation by Nsp15. The mRNA degradation assay confirmed several hits inhibiting 100% of Nsp15 activity and reduced the collection above to 308 (a confirmed hit rate of 11.6%, higher than 5% hit rate shown by fragment-based drug-discovery approach[27]). To narrow down the hit number for potent covalent inhibitors, all three assays were repeated at a second concentration of 10 μM. This further reduced the count to 60 compounds (a hit rate of 2%). Sixty compounds were repurchased and validated using all three assays at a concentration of 40 and 10 μM, and this resulted in the identification of 15 covalent inhibitors against Nsp15. Finally, a dose response fluorescent-based assay that used an RNA substrate[13] was performed to validate and select potent inhibitors. This assay validated 10 compounds with IC_{50}s less than 5 μM (Fig. 1B and S1†).

Acrylamide based Nsp15 inhibitors are non-toxic

We assessed the thiol reactivity of the top electrophile hits by incubating with reduced Ellman's reagent (5,5-dithio-bis-2-nitrobenzoic acid (DTNB)), and followed the absorbance of TNB^{2-} at 412 nm wavelength for up to 5 hours[28] (Fig. 2A). To measure the kinetic constants and evaluate the intrinsic reactivity of these acrylamide-based Nsp15 inhibitors towards thiols, we fitted the data to a second-order reaction rate

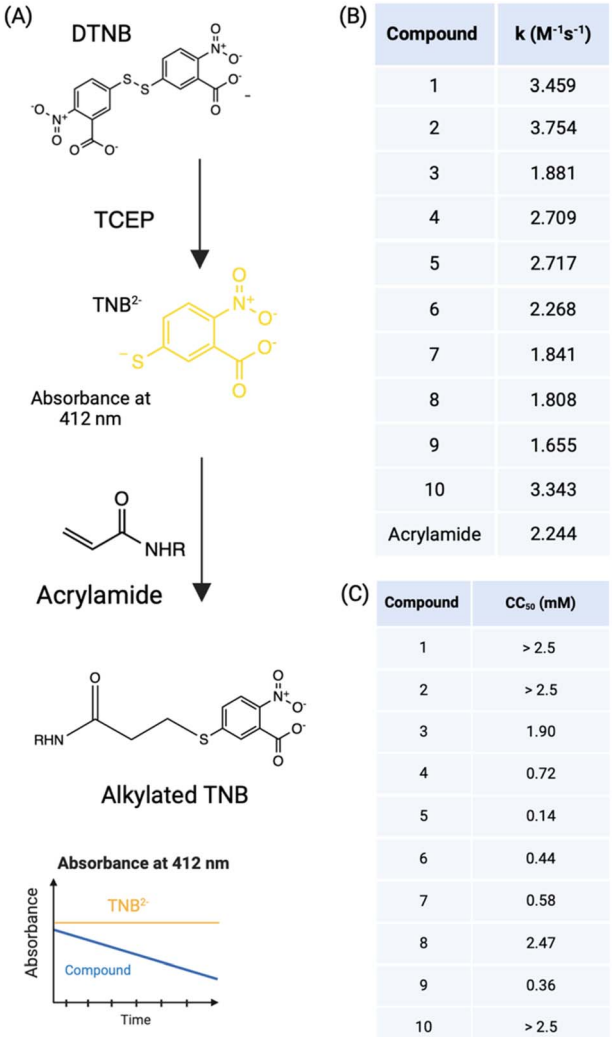

(B)

Compound	k ($M^{-1}s^{-1}$)
1	3.459
2	3.754
3	1.881
4	2.709
5	2.717
6	2.268
7	1.841
8	1.808
9	1.655
10	3.343
Acrylamide	2.244

(C)

Compound	CC_{50} (mM)
1	> 2.5
2	> 2.5
3	1.90
4	0.72
5	0.14
6	0.44
7	0.58
8	2.47
9	0.36
10	> 2.5

Fig. 2 Acrylamide based inhibitors have moderate non-specific reactivity with thiols and are non-toxic to mammalian cells. (A) Scheme for determining thiol reactivity of Nsp15 covalent inhibitors (200 μM) using Ellman's reagent; (B) the kinetic rate constant of alkylation of TNB^{2-} by acrylamide-based inhibitors (k) (M^{-1} s^{-1}) was calculated and compared with acrylamide; (C) a cell viability assay utilizing the dye resazurin was performed with different concentrations (0–0.5 mM) of inhibitors and revealed the compounds to be non-toxic at the doses tested. The cytotoxic concentration 50% (CC_{50}) (mM) is shown in the table for Caco-2 cells.

equation and extrapolated the kinetic constant for the alkylation by the acrylamide-based inhibitors. All compounds showed an excellent fit to the kinetic model of one-phase exponential decay (R^2 > 0.9). The kinetic rate constant (k) for Nsp15 inhibitors ranged from 1.5–4 M^{-1} s^{-1} (Fig. S2†).

Next, we assessed drug toxicity, which is a key parameter in clinical pharmacology and routinely performed during preclinical screening of drug candidates.[29] To assess the drug response and toxicity, a resazurin assay was used to analyze the cell viability[30] in response to Nsp15 inhibitor compound treatment. A range of concentrations (0.03–0.5 mM) of inhibitors was tested on Caco-2 cells (*in vitro* model of the intestinal epithelial cells), and cell viability was measured and the CC_{50} was calculated (Fig. 2C). At the lower concentrations (0.3–0.125 mM), most of the compounds (except compound **5**) showed 100% cell viability, suggesting no toxicity at the tested concentrations. At the higher concentration (0.25–1 mM), compounds 1, 2, 3, 8 and 10 show cell viability greater than 85%, while the rest showed less than 40% viability, indicative of some negative effects on cell viability.

Acrylamide-based inhibitors show specificity and are active towards Nsp15 from other coronaviruses

Nsp15 is an evolutionary conserved protein and considered as a genetic marker for nidoviruses. Conservation of Nsp15 across species suggests that SCoV-2 Nsp15 inhibitors might be also used to target Nsp15 from other coronaviruses. SCoV-2 Nsp15 shares sequence identity with other coronavirus species such as SCoV-1, and Middle East respiratory syndrome coronavirus (MERS-CoV), with corresponding percentages of 88.44% and 51.47%, respectively (Fig. S3A†).[16] We wondered if these ten compounds could also inhibit Nsp15 from SCoV-1 and MERS-CoV. To examine this, we tested the inhibitory activity of these compounds against Nsp15 from SCoV-2, SCoV-1 and MERS-CoV using a fluorescent based endonuclease assay. We observed that compounds inhibited SCoV-1 and MERS-CoV Nsp15 to varying extents. A dose response assay was performed to determine the IC_{50} values of these compounds against Nsp15 from SCoV-2, SCoV-1 and MERS-CoV (Fig. 3A and S3B). Since several inhibitors were able to work on other viral variants, we assert that these acrylamide compounds could serve as useful initial hits for development into second-generation compounds against other coronaviruses.

To examine the broad specificity of the compounds, we also tested these ten compounds against a distantly related RNA endonuclease, RNase A that shares a similar catalytic mechanism with Nsp15. We observed that none of the inhibitors inhibited RNase A activity, suggesting the inhibitors are not acting through the conserved catalytic triad, as expected (RNase A and Nsp15 share the catalytic triad). We also tested these compounds against an unrelated enzyme SIRT1, that has been implicated for modifications (transnitrosation, glutathionylation) of cysteine residue as a mechanism of its physiological inhibition. As expected, and hypothesized, none of the compounds inhibited SIRT1 enzymatic activity, suggesting the nucleophilic cysteine in SIRT1 was not being alkylated by acrylamide based Nsp15 inhibitors. The statistical analysis, *t*-test of DMSO with each compound (compound **1–10**) resulted in a *p*-value greater than 0.05 (p > 0.05), suggesting no significant difference in enzymatic activity. Together, these results demonstrate that these acrylamide-based compounds are relatively specific inhibitors that act on Nsp15 from various coronaviruses (Fig. 3B).

Ability of acrylamide-based inhibitors to inhibit Nsp15 in cells

To assess the inhibitory effect of these *in vitro* Nsp15 inhibitors in a cellular environment, we utilized a live virus infection assay based on a genetic ablation of Nsp15 activity resulting in a higher production of IFN-β during Nsp15 mutant virus

(A)

Compound	SCoV-2 (IC_{50}(μM))	SCoV-1 (IC_{50}(μM))	MERS-CoV (IC_{50}(μM))
1	3977	5129	1375
2	533	7876	1682
3	0.368	25.46	15.53
4	0.596	117.2	40.74
5	12.77	952.6	361.6
6	0.496	23.32	17.96
7	0.420	88.18	36.48
8	6.8	508.3	167.6
9	0.383	23.36	17.86
10	8.415	189.4	107.0

(B)

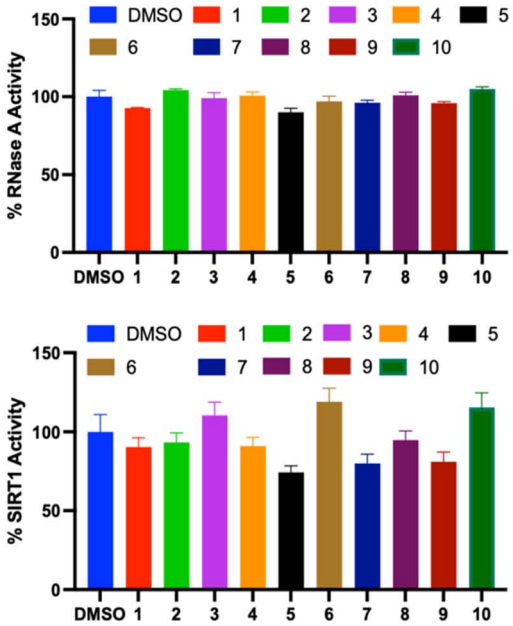

Fig. 3 Acrylamide based inhibitors show specificity towards Nsp15 from coronaviruses. (A) A dose response assay determining IC_{50}s of ten inhibitors against Nsp15 from SCoV-2, SCoV-1 and MERS-CoV demonstrated that these inhibitors could also be utilized as initial hits for other coronaviruses; (B) effect of inhibitors on unrelated proteins, RNase A and SIRT1 show their specificity towards Nsp15. Results are expressed as percent activity relative to the DMSO control and were normalized based on quenching effects of the compounds in the respective assays using control substrates. Mean ± SD is shown ($n = 3$ independent experiments).

infection.[8] With a catalytic-inactive mutant (H234A) of Nsp15 as a positive control, we evaluated ten compounds in the Caco2-AT culture system. All the compound-treated cells did not produce more IFN-β compared to the untreated wild-type (WT) group, and some even produced less than the WT group. We found that the viral nucleocapsid (N) gene levels of all tested samples were comparable, indicating that all the cells were successfully infected (Fig. S4†). These results suggest that these ten compounds show no significant inhibitory effect on Nsp15 activity during SCoV-2 infection in the Caco2-AT test system. The lack of inhibitory effect might be due to their relative low potency (high IC_{50}) of the compounds.

Nsp15 covalent inhibitors are predicted to have favorable drug-like properties

Estimation of the pharmacokinetic profile of a drug candidate is a crucial aspect in drug development that includes parameters like its absorption, distribution, metabolism, and excretion (ADME).[31] In this report, we carried out theoretical prediction of ADME parameters of the inhibitors using SwissADME,[32,33] a free and readily accessible web tool. We predicted the physiochemical properties, pharmacokinetics, drug-likeness, and medicinal chemistry friendliness of these small molecules by importing their 2D structures into a webpage interface using the canonical simplified molecular input line entry system (SMILES) format.

The ability of a drug to move across the membranes for transportation throughout the body is highly dependent on its physiochemical properties.[34,35] All the Nsp15 inhibitors identified had optimal values for their physiochemical properties, indicating they should have good oral bioavailability, suggesting them as promising drug candidates[36] (Fig. S5A†). SwissADME can also predict gastrointestinal (GI) absorption and blood–brain barrier (BBB) penetration,[37] two pharmacokinetic behaviors associated with lipophilicity and polarity of the molecules. While all acrylamide based Nsp15 inhibitors were predicted to have a high level of GI absorption, six out of ten inhibitors showed a probability of crossing the BBB. Interestingly, all the inhibitors were deemed to be non-substrates of P-glycoprotein (P-gp), suggesting that they are unlikely to be effluxed from cells.

Drug-likeness is an essential aspect of drug development that evaluates the potential of a molecule to become an oral drug.[38] These ten inhibitors followed Lipinski's rule of five,[39] with zero violations and a bioavailability score of 0.55, displaying good bioavailability and demonstrating a similarity to other successfully developed oral drug candidates (drug-likeness).[40] Importantly, the Nsp15 inhibitors identified herein did not show any PAINs alerts, as indicated by a score of zero. The ease with which these compounds can be synthesized is another positive consideration for their use as lead compounds (Fig. S5B†). To validate these results, we confirmed the drug likeness of these ten compounds using ADMETlab2.0.[41]

Compound 10 modifies a cysteine in the C-terminal domain of Nsp15

To determine the cysteine residue(s) that mediate the covalent interaction between Nsp15 and the compounds, we performed

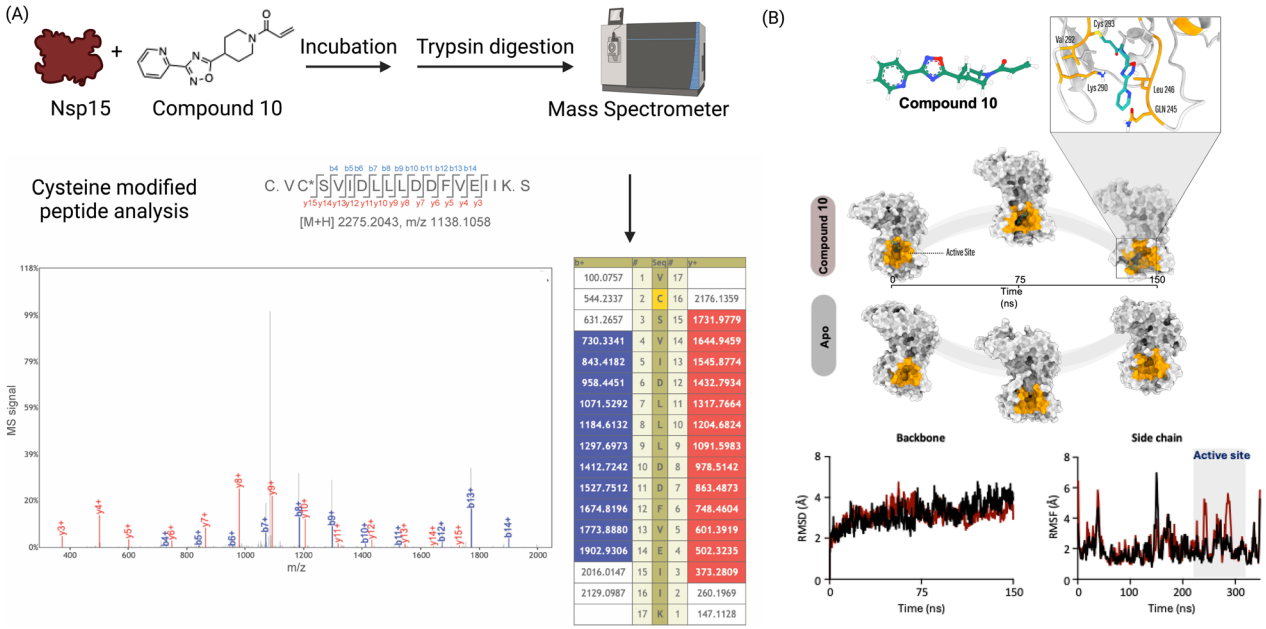

Fig. 4 Compound **10** modifies Cys293 in Nsp15 and distorts the active site in the C-terminal domain of Nsp15. (A) Compound **10**–Nsp15 was subjected to trypsin digestion followed by LC-mass spectrometry and analyzed by shotgun analysis. A peptide with Cys293 was found to be modified with compound **10**; (B) structural analysis from the MD simulations of 150 ns of compound **10**–Nsp15 complex in comparison to apo Nsp15 revealed that the irreversible binding of compound **10** to Nsp15 significantly distorts the active site.

tandem mass spectrometry (MS/MS) analysis of protein–compound adducts subjected to trypsin digestion. Tandem mass spectrometry revealed that compound **10** is covalently reacting with Cys293. Cys293 is present in the C-terminal domain of Nsp15, next to the catalytic core of Nsp15 harboring endoribonuclease activity.[42] Cys293 has been also been implicated in interaction with the drug Favipiravir through van der Waals interactions in molecular docking simulations[43] (Fig. 4A).

To assess the structural dynamics of Nsp15 following the irreversible covalent reaction of compound **10** to Cys293, we conducted molecular dynamics (MD) simulations of Nsp15 in its apo form and in complex with compound **10** (covalently bound to Cys293). Structural analysis from the MD simulations revealed that the irreversible binding of compound **10** to Nsp15 significantly distorts the active site (Fig. 4B). Although there is no observable change in the overall backbone of Nsp15, the side chain fluctuations in the compound **10**-bound complex are altered, indicating a distortion of the binding site.

Development of an AI model to support Nsp15 hit-to-lead optimization

During drug discovery, turning an early stage hit molecule into a nanomolar-range lead molecule often requires numerous iterations, and even then, it carries a significant chance of failure. Therefore, to expedite this process, we utilized the power of AI to identify distinguishing characteristics between the successful and unsuccessful Nsp15 inhibitors in our library, an endeavor that would be impossible to be achieved manually. To the best of our knowledge, we are the first group to leverage AI for the screening of SCoV-2 Nsp15 inhibitors. Thus, we utilized our experimental HTS data to train sophisticated AI models to streamline the hit-to lead discovery process and make it less laborious and expensive (Fig. 5A). Our AI-driven methodology demonstrated a marked improvement in prediction accuracy and has the potential to reduce false positives and negatives.

Artificial intelligence requires a vast training dataset comprising millions of data points; however, it is next to impossible to generate an experimental dataset this large in drug discovery. Effective training of AI models cannot be achieved with smaller dataset. Therefore, to overcome this challenge, we explored several strategies, including fine-tuning large language models, applying prompt engineering for ChatGPT-based predictions, and combining embeddings from language models with traditional machine learning techniques. We used various AI models, including Random Forest (RF), SVM, Random Forest (RF), Decision Tree (DT), Gradient Boosting (GB), Logistic Regression (LR), Naïve Bayes (NB), KNN, C4.5, Convolutional Neural Networks (CNNs), Recurrent Neural Networks (RNNs), LLMs models such as GPT-3.5-turbo, and GPT-4-turbo. Each of these models was optimized and fine-tuned to enhance accuracy and precision. Among these, the Gradient Boosting model demonstrated the best performance, as shown in Fig. S6A.†

We extensively experimented with different algorithm parameters and input features to improve model accuracy. For the machine learning models, we utilized a grid search approach to find the best hyperparameters for each model. We evaluated various LLM models for inhibitor prediction. After extensive testing and optimization of the models, we developed our model, which integrates Gradient Boosting and LLM. This

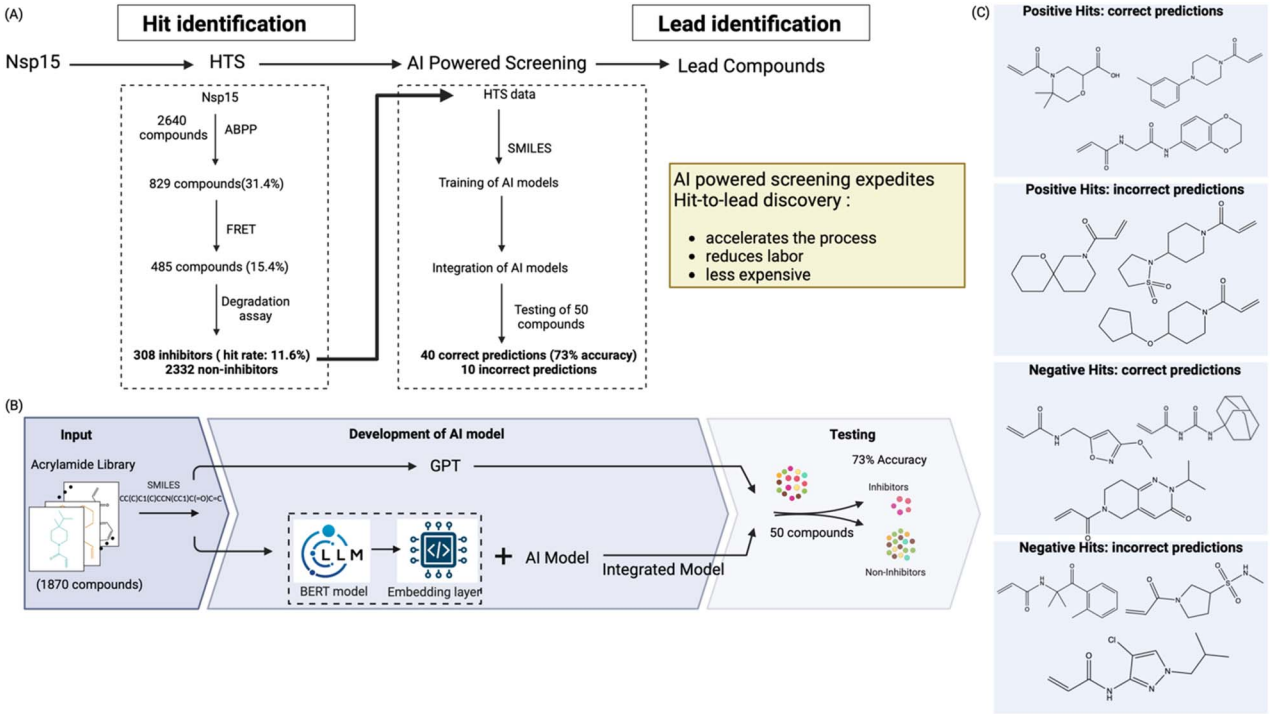

Fig. 5 Development of an AI model to predict Nsp15 inhibitors and accelerate the process of hit to lead identification. (A) The results from the high throughput screening assay against Nsp15 were used to develop an AI model that could virtually screen thousands of compounds to predict inhibitors and non-inhibitors against Nsp15; (B) the AI model was developed by utilizing the chemical properties, integrating ChemBERTa, and machine learning techniques to predict Nsp15 inhibitors. The integrated model was tested on 50 unlabeled compounds, and its ability to predict inhibitors was determined. The model showed 73% accuracy in distinguish inhibitor from non-inhibitors; (C) representation of the test predictions made by the integrated AI model. The rest of the compounds are shown in Fig. S6B.†

model combines features and embedding vectors from the LLMs to train a new model for predicting inhibitors from a pool of chemical structures (Fig. 5B).

We measured the model's performance using four main metrics: recall, precision, F1 score, and efficiency. Recall checks how well the model finds all the correct results, which is important to avoid missing key compounds. Precision looks at how many of the positive predictions are actually correct, helping reduce false alarms. The F1 score combines recall and precision into one measure to give a balanced view of performance, especially when the data is uneven. Efficiency measures how quickly and easily the model makes predictions, which is important for real-time or large-scale use. Together, these metrics show how well the model works and where it can improve. The efficiency for all the individual models was greater than 50%, suggesting that our proposed pipeline is effective in dealing with small datasets for inhibitor prediction. This integrated approach significantly improved prediction accuracy, showing a precision value of 0.73 and an F1 score of 0.73, further indicating its high accuracy.

To validate our model, we tested it on an existing Nsp15 inhibitor data set, recently published.[44] Our model predicted 9 out of 12 inhibitors listed in this recently published paper correctly, demonstrating its high accuracy. After validation, we employed our Integrated AI model to test 50 unlabeled compounds. This model predicted the unlabeled inhibitors with an accuracy of 73%. All the correct and incorrect predictions made on these 50 test compounds are presented in Fig. 5C and S6B.† Moving forward, we anticipate that this experimental-led AI driven experimental discovery platform will identify new potent lead compounds in a cheap and efficient manner. Moreover, the platform we present here can also be adapted for the discovery of inhibitors for other high-value target proteins.

Experimental

Materials and methods

Expression and purification of SCoV-2 Nsp15. The plasmid expressing SCoV-2 Nsp15 (6×-His-Thrombin-TEV-Nsp15 in pET-14b vector) was a kind gift from Robin Stanley, NIH. SCoV-2 Nsp15 was expressed as described in Pillon *et al.*[13] Briefly, the plasmid was transformed into C41 (DE3) competent cells and selected on carbenicillin LB agar plates. Next day, a colony was picked to grow primary culture of 10 mL 2XYT media supplemented with 50 μg per mL carbenicillin. The secondary culture was grown by diluting primary culture 1 : 100 in 2XYT media to an OD of 1.0 (A_{600}). SCoV-2 Nsp15 protein was expressed with 0.2 M isopropyl β-D-1-thiogalactopyranoside (IPTG) for 3 hours at 37 °C. The culture was harvested and resuspended in lysis buffer (50 mM Tris pH 8.0, 500 mM NaCl, 5% glycerol) supplemented with EDTA-free protease inhibitor tablets. The cells were sonicated, and lysate was clarified at 13 000×*g* for 30 minutes at 4 °C. The supernatant was loaded on Talon HP

column (Cytiva) at the speed of 1 mL min^{-1}. The non-specific protein was removed by washing the column with lysis buffer supplemented with 10 mM imidazole. Nsp15 was eluted with high imidazole buffer (lysis buffer supplemented with 250 mM imidazole). The eluted fraction of Nsp15 were pooled, concentrated, and dialyzed against SEC buffer (20 mM HEPES pH 7.3, 150 mM NaCl, 5 mM $MnCl_2$, 5 mM beta-mercaptoethanol (β-me)). The protein was stored in −80 °C until further use.

SCoV-1 and MERS-CoV Nsp15 variants were purified as previously described.[16] Briefly, BL21(DE3) pLYsS cells were transformed with pet28B+ plasmids encoding for these Nsp15 variants. Starter cultures were grown overnight at 37 °C in terrific broth (TB) in the presence of 100 μg mL^{-1} kanamycin. Larger cultures of TB-kanamycin were inoculated with starter culture and grown to an OD 600 nm of 0.6. Cultures were then cooled at 4 °C for 30 minutes before induction with 1 mM IPTG at 16 °C for 20 hours. Cells were then pelleted at 6000×*g* for 20 minutes at 4 °C and resuspended in lysis buffer (20 mM Tris pH 8.0, 150 mM NaCl, 5 mM imidazole, 0.1% Triton X-100, 1 mg mL^{-1} lysozyme) supplemented with EDTA-free Roche Complete Ultra protease inhibitor tablet (Sigma), 1 mM PMSF and 1 mM β-me. The lysate was incubated on ice for 30 minutes before sonication with a Branson Digital Sonifier at 25% amplitude (15 seconds on, 1 minute off) for 10 pulses. Debris was pelleted *via* centrifugation at 20 000×*g* and the clarified lysate was incubated with Ni-NTA beads (Qiagen) at 4 °C for 4 hours with gentle rotation. The beads were washed in 20 mM Tris pH 8.0, 300 mM NaCl, 10 mM imidazole, 0.01% Triton X-100, and 1 mM β-me. The proteins were eluted by incubating the beads with 10–250 mM imidazole. Fractions were analyzed for purity *via* SDS-PAGE and staining with Coomassie Brilliant Blue R-250 (Bio-Rad). Pooled fractions were concentrated with a Pierce Protein concentrator 10K (Thermofisher). The buffer was exchanged during concentration with 20 mM HEPES pH 7.5, 150 mM NaCl, 0.1 mM DTT, and 10% glycerol. Concentrated protein was aliquoted and stored at −80 °C until usage. Protein concentration was measured using the DTT-resistant Pierce 660 nM Protein BCA Assay kit (Thermofisher).

Activity based protein profiling to find cysteine binders. The cysteine-reactive compounds against Nsp15 were identified using competitive gel-based ABPP. An iodoacetamide-rhodamine (IA-Rho) probe was used to alkylate cysteines within Nsp15 and can be competed out by covalently bound compounds from pre-treatment. In the total reaction volume of 25 μL, 0.25 μg of Nsp15 was incubated with 40 or 10 μM of the compound for 30 minutes at 37 °C. In the absence of compound, DMSO was added as a negative control. After incubation, 0.5 μM of IA-Rho was added and incubated for 30 minutes in the dark at room temperature. The reaction was stopped using 10 μL of SDS loading buffer, boiled for 5 minutes at 95 °C and 12.5 μL of the sample was loaded on tris-glycine gel. The gel was imaged under rhodamine fluorescence. Cysteines within Nsp15 that have been covalently modified would not be labeled by IA-Rho, leading to a reduction in signal on the gel.

Chemical library composition and liquid handling. The electrophilic covalent probe library purchased from Enamine was stored at 10 mM and 2 mM in DMSO in 384-well master plates (Greiner Cat # 784201). Primary screening plates (Corning Cat # 3573) were generated using a Cybio Well Vario liquid handler (Analytik Jena, Jena, Germany) from 2 mM plate to yield a final concentration of 40 μM or 10 μM compound with a DMSO concentration of 2% (v/v). Hits were cherry picked from master plates and re-arrayed onto new masters with a Tecan Freedom Evo 150 (Tecan Systems Inc, San Jose, CA) at the Drug Discovery Center, UC Berkeley.

Fluorescent assay to determine the Nsp15 inhibitors. The fluorescent based Nsp15 activity assay was optimized in 384-well plate (Corning Cat# 3573). The DNA–RNA hybrid substrate (5′FAM-dArUdAdA-TAMRA-3′) was custom ordered from Creative Biogene. The final reaction volume of 25 μL consisted of 12.5 μL of Nsp15 protein (5 nM) and Nsp15 substrate (1 μM) diluted in cleavage buffer (20 mM HEPES pH 7.5, 100 mM NaCl, 5 mM $MnCl_2$) with 2% DMSO (absence and presence of compound (40 and 10 μM)). The Nsp15 activity was monitored by measuring fluorescent intensity at given wavelengths (excitation: 485 nm and emission: 535 nm) after 1 hour. The data was analyzed in CDD vault analysis servers. The dataset was normalized to the baseline (negative control: in absence of Nsp15) and activity response (positive control: in presence of Nsp15) and calculated as percentage inhibition using GraphPad Prism. The dose response assay was performed to determine the IC_{50}s. The experiments were run in duplicates.

mRNA degradation assay to discover the Nsp15 inhibitors. In mRNA degradation assay, 500 ng of Nsp15 was incubated with compound (40 and 10 μM) (2% DMSO in the absence of compound) for 30 minutes in the 25 μL of the buffer (20 mM HEPES pH 7.3, 100 mM NaCl, 5 mM $MnCl_2$) at room temperature. After incubation, the Fluc mRNA (0.3 μg) (TriLink Biotechnologies) was added to the pre-incubated Nsp15 and allowed the degradation of mRNA for 30 minutes. The RNA loading dye was added and ran on 1% agarose gel. The negative control (mRNA in the absence of Nsp15 and compounds) was also included. The compounds that prevented the mRNA degradation were taken as Nsp15 inhibitors.

Validation of Nsp15 inhibitors. The Nsp15 inhibitors obtained from three sequential assays were validated, and dose–response assay was performed to determine IC_{50} using fluorescent assay, The enzyme assays were performed in triplicates at 25 °C using a 96-well plate. The compounds (1 μL in 100% DMSO at the final concentrations ranging from 30 nM to 800 μM in a 50 μL reaction) were preincubated with 4 nM hexameric Nsp15 in a 30 μL buffer A (20 mM HEPES pH 7.2, 100 mM NaCl, 5 mM $MnCl_2$) for 30 minutes. The final concentration of DMSO was 3.3%. Then, 20 μL of 0.5 μM RNA substrate (5′6-FAM-AAAUAA-3′6-TAMRA, GenScript) in a buffer A was added to the protein–compound complex and fluorescent intensity was measured at excitation/emission wavelength of 485/528 every 5 min for 120 minutes. The IC_{50} values were calculated based on the final concentrations of the compounds at the 45- or 90-minutes time points using GraphPad Prism.

Specificity assay

Nsp15 and RNase A activity assay. An adapted FRET-based assay was used as previously described[42] employing an RNA

substrate with the sequence: 5′FAM-CAACUAAACGAAC-BHQ1′3 where FAM and BHQ1 are 6-Carboxyfluorescein and Black Hole Quencher respectively. The reactions were done in black 96-well polystyrene plates (Greiner, Bio-One) in a 60 μL volume. The reactions contained 60 ng of protein, 1× reaction buffer (25 mM HEPES pH 7.3, 50 mM NaCl, 5 mM $MnCl_2$), and various concentrations of compounds all dissolved in DMSO and were preincubated together in the dark for 30 minutes at RT. RNA substrate was then added to a final concentration of 1 μM and plates were incubated at 37 °C for a further 20 minutes. Fluorescence data was collected using a Varioskan LUX plate reader using excitation and emission wavelengths of 495 and 520 nm respectively. The results shown are the average of 3 biological replicates ± SD.

SIRT1 fluor de lys activity assay. SIRT1 activity was measured using the FLUOR DE LYS® SIRT1 fluorometric drug discovery assay kit (Enzo Life Sciences). Recombinant SIRT1 was purified as described in the protein purification methods above.[45] SIRT1, FdL substrate, and NAD^+ were used at final concentrations of 200 nM, 25 μM, and 5 mM, respectively. Inhibitor compounds were preincubated with SIRT1 in the absence of NAD^+ or FdL Substrate for 30 minutes at 25 °C. The reactions were then allowed to proceed for 30 minutes at 37 °C following the addition of substrate. The reactions were terminated by the addition of developer reagent and incubated for 15 minutes at room temperature in the dark before being measured on a spectrophotometer using excitation and emission wavelengths of 360 and 460 nm, respectively on a Varioskan LUX plate reader. The results shown are the average of 3 biological replicates ± SD.

Cell lines and virus. A Caco-2 cell line expressing hACE2 and hTMPRSS2 (Caco2-AT),[46] a gift from Dr Mohsan Saeed (Boston University), was propagated in DMEM containing 10% FBS, 1% Pen/Strep, 1× NEAA, 1 μg per mL puromycin (InVivogen, ant-pr-05), and 1 μg per mL blasticidin (InVivogen, ant-bl-05). A Vero E6 line expressing hACE2 and hTMPRSS2 (Vero-AT) was obtained through BEI Resources, NIAID, NIH, and maintained in DMEM containing 10% FBS, 1% Pen/Strep, 1× NEAA, 1 μg mL per puromycin (InVivogen, ant-pr-05).

The following SCoV-2 strain/isolate was obtained through BEI Resources, NIAID, NIH: Washington strain 1 (WA1) (NR-52281). A recombinant virus expressing catalytic-inactive Nsp15 (Nsp15mut) was generated using an infection clone as described here.[47] These viruses were propagated once with Vero-AT cells to obtain large viral stocks and were titrated with Vero-AT cells.

Assessment of Nsp15 activity inhibition with live SCoV-2. The evaluation of the inhibitory effect of Nsp15 inhibitors against live SCoV-2 was conducted in a certified BSL-3 lab at Oklahoma State University. Caco2-AT cells (3.0×10^5 cells per well) were seeded in 12-well plates a day prior to infection. The work concentrations of the compounds were determined as follows based on a cell viability assay: compounds 1, 2 and 10 at 0.5 mM; compounds 3, 5, 7, and 9 at 0.1 mM; compounds 4 and 8 at 0.2 mM; and compound **5** at 0.05 mM. Cells in the 12-well plates were infected with the indicated viral strains at a multiplicity of infection (MOI) of 0.1 in serum-free media for 1 hour. After incubation, the inoculum was removed, and 1 mL of diluted compound and 2 μM p-glycoprotein inhibitor CP-100356 were added to each well. After 48 hours of incubation at 37 °C, the cell culture supernatants were removed, and the cells were collected in Qiagen RLT lysis buffer (Qiagen, Hilden, Germany).

RNA extraction and real-time PCR quantification. RNA was extracted from the Caco2-AT cells using RNeasy Mini kit (QIAGEN, 74106) following the manufacture's protocol. 1 μg of RNA was converted to cDNA by using RT2 HT First Strand Kit (QIAGEN, 330411) which contains a component to eliminate genomic DNA contamination. Quantitative PCR was performed with specific primers (Table S1†) using PowerUp SYBR Green Master mix (Fisher, A25918) on QuanStudio 6 Pro (ThermoFisher, A43160). Cycle threshold values were normalized to 18S rRNA levels by using the $2^{-\Delta Ct}$ method. The forward and reverse primers for human IFN-β gene were CTTGGATTCCTACAAAGAAGCAGC and TCCTCCTTCTGGAACTGCTGCA, respectively. The forward and reverse primers for SCoV-2 N gene were AAGCTGGACTTCCCTATGGTG and CGATTGCAGCATTGTTAGCAGG, respectively.

Mass spectrometry

1D method. Mass spectrometry was performed at the Proteomics/Mass Spectrometry Laboratory at University of California, Berkeley. A nano LC column was packed in a 100 μm inner diameter glass capillary with an integrated pulled emitter tip. The column consisted of 10 cm of Polaris c18 5 μm packing material (Varian). The column was loaded and conditioned using a pressure bomb. The column was then coupled to an electrospray ionization source mounted on a Thermo-Fisher LTQ XL linear ion trap mass spectrometer. An Agilent 1200 HPLC equipped with a split line to deliver a flow rate of 1 μL min^{-1} was used for chromatography. Peptides were eluted with a 90-minute gradient from 100% buffer A (5% acetonitrile/0.02% heptafluorobutyric acid (HBFA)) to 60% buffer B (80% acetonitrile/0.02% HBFA). Collision-induced dissociation and electron transfer dissociation spectra were collected for each *m*/*z*. Protein identification, quantification, and analysis were done with Integrated Proteomics Pipeline-IP2 (Bruker Scientific LLC, Billerica, MA, http://www.bruker.com) using ProLuCID/Sequest,[48,49] DTASelect2,[50,51] and Census.[52,53] Spectrum raw files were extracted into ms1 and ms2 files from raw files using RawExtract 1.9.9 (http://fields.scripps.edu/downloads.php) 10, and the tandem mass spectra were searched against Nsp15.

LC/MS–MS mapping of modified peptides. Trypsin/Lys-C digested peptides were analysed by online capillary nanoLC-MS/MS using a 25 cm reversed phase column fabricated in-house (75 μm inner diameter, packed with ReproSil-Gold C18-1.9 μm resin (Dr Maisch GmbH)) that was equipped with a laser-pulled nanoelectrospray emitter tip. Peptides were eluted at a flow rate of 300 nL min^{-1} using a linear gradient of 2–40% buffer B in 140 min (buffer A: 0.02% HFBA and 5% acetonitrile in water; buffer B: 0.02% HFBA and 80% acetonitrile in water) in an Thermo Fisher Easy-nLC1200 nanoLC system. Peptides were ionized using a FLEX ion source (Thermo

Fisher) using electrospray ionization into a Fusion Lumos Tribrid Orbitrap Mass Spectrometer (Thermo Fisher Scientific). Data was acquired in orbi-trap mode. Instrument method parameters were as follows: MS1 resolution, 120 000 at 200 m/z; scan range, 350−1600 m/z. The top 20 most-abundant ions were subjected to collision-induced dissociation with a normalized collision energy of 35%, activation q 0.25, and precursor isolation width 2 m/z. Dynamic exclusion was enabled with a repeat count of 1, a repeat duration of 30 seconds, and an exclusion duration of 20 seconds. RAW files were analysed using PEAKS (Bioinformatics Solution Inc.) with the following parameters: semi-specific cleavage specificity at the C-terminal site of R and K, allowing for 5 missed cleavages, precursor mass tolerance of 15 ppm, and fragment ion mass tolerance of 0.5 daltons. Methionine oxidation was set as variable modifications and cysteine carbamidomethylation was set as a fixed modification. Peptide hits were filtered using a 5% FDR. Proteins with at least 2 unique peptides were filtered with a 5% FDR. Label free quantitation (LFQ) was performed using PEAKS quantitation module and default parameters with the following exceptions: top 2 peptides for each protein with a min of 10XE4 abundance was used and the TIC was used for all normalization including technical replicates.

Molecular modelling. The crystal structure of Nsp15 was obtained from the Protein Data Bank (PDB ID: 6WXC).[15] The protein structure was prepared using the Maestro Schrödinger Protein Preparation Wizard. The co-crystallized ligand was removed, and water molecules located more than 5 Å away from the protein residues were removed, missing side chains were added, and the pK_a of the ionizable groups was set to 7.4 using PROPKA.[54] The protein then underwent restrained minimization and was placed inside an orthorhombic box. Water molecules (TIP3P) were added with a 10 Å buffer. The simulations were performed under the NPT ensemble to maintain a constant temperature and pressure, set at 300 K and 1.01325 bar, respectively, for 150 nanoseconds using the OPLS3 force field.[55] Separately, ligand molecules were prepared using the LigPrep module and then covalently bonded to cys293. The simulation outputs were analyzed using the Schrödinger Maestro suite, with graphical representations created using ChimeraX.[56,57]

Drug-likeness evaluation. A list of SMILES of Nsp15 inhibitors that have IC_{50} less than 5 μM were submitted to a freely accessible web tool at SwissADME (**http://www.swissadme.ch**) and run.

Optimization of AI models. The code for the models that we trained in this paper is available here **https://github.com/bmosavati/AI-Powered-Platform-Drug-Discovery**.

Dataset and feature engineering. In this study, we utilized machine learning and artificial intelligence models to investigate the inhibitory potential of acrylamide fragments on the non-structural protein 15 (Nsp15) of the SCoV-2 virus. Chemical compounds were represented using SMILES notation. To ensure high-quality data, the dataset underwent a comprehensive cleaning and preprocessing process. Compounds with incomplete or invalid SMILES strings were excluded to eliminate errors in data representation. Duplicate entries were removed to avoid redundancy and missing molecular descriptor values were addressed by excluding entries with significant gaps to maintain data integrity. Additionally, oversampling techniques were employed to correct the class imbalance between the minority class (Nsp15 inhibitors) and the majority class (non-inhibitors). These steps ensured a balanced dataset, improving model robustness and the reliability of machine learning predictions. The MACCS fingerprint method was employed to convert SMILES strings into a format suitable for machine learning. The MACCS method generates 166 binary bits, each representing the presence or absence of specific chemical substructures or features. In addition to the MACCS fingerprints, we incorporated ten molecular descriptors into our dataset: molecular weight, log P (MolLog P), number of atoms, number of bonds, number of rings, rotatable bond counts, hydrogen bond donors, hydrogen bond acceptors, number of stereocenters, and topological polar surface area (TPSA). These features were normalized prior to their integration into the dataset. The dataset comprised 1920 entries, including 257 molecules identified as Nsp15 inhibitors (positive hits), 1613 molecules with no inhibitory action against Nsp15 (negative hits). The dataset was divided into training, validation, and testing sets with a 70%, 15%, 15% split: specifically, 70% (1309 compounds) for training, 15% (280 compounds) for validation, and 15% (280 compounds) for testing, and 50 molecules reserved for validation purposes as unlabeled compounds.

Machine learning and deep learning models. We employed a variety of machine learning algorithms to train, test, and predict the inhibitory potential of the compounds. These algorithms included Logistic Regression, Decision Tree, Support Vector Machine (SVM), Naive Bayes, Gradient Boosting, K-Nearest Neighbors (KNN), and Linear Regression (LR).[58–60] Additionally, we utilized deep learning models such as Convolutional Neural Networks (CNNs), Recurrent Neural Networks (RNNs).[61–63] Large Language Models (LLMs), including GPT-3.5, GPT-4, and ChemBERT, were also leveraged for classification tasks. Model performance was evaluated using metrics such as accuracy, precision, and F1-score.

ChemBERTa-based models

Fine-tuning ChemBERTa on SMILES strings. We fine-tuned the ChemBERTa model, which is specialized in handling chemical structures represented as SMILES strings. The pre-trained ChemBERTa model was augmented with a fully connected layer followed by a classifier layer.[64–67] This fine-tuning process involved adjusting the learning rates, dropout rates, and the number of training epochs to enhance model performance specifically for predicting Nsp15 inhibitors. The fine-tuned model was solely trained on the SMILES strings from our dataset to capture intricate chemical structure representations.

Integrating SMILES embeddings with molecular descriptors. In another approach, we extended the use of ChemBERTa by integrating additional molecular descriptors with SMILES embeddings. Initially, SMILES strings were embedded using the pre-trained ChemBERTa model. These embeddings were then

concatenated with normalized quantitative features such as molecular weight, log *P*, and other relevant descriptors. The combined embeddings and features were passed through a dropout layer to mitigate overfitting risks and subsequently fed into a dense layer for final predictions. This integration aimed to leverage both chemical structure information and specific molecular properties to improve prediction accuracy.

Utilizing ChemBERTa for sequence embeddings in traditional ML models. We also explored the use of ChemBERTa purely for generating sequence embeddings of SMILES strings. These embeddings, representing detailed chemical structure information, were extracted, and then utilized as input features in traditional machine learning models. The machine learning algorithms employed included Logistic Regression, Decision Tree, SVM, Naive Bayes, KNN, GB and Linear Regression. This method allowed us to compare the efficacy of deep learning-based embeddings against traditional fingerprint-based approaches.

GPT-based models. GPT models were employed to classify molecules based solely on their SMILES strings. We tested three variations of prompts: one containing only SMILES strings, another including both SMILES strings and the protein sequence of Nsp15, and a third combining SMILES strings with small molecule features. Due to GPT's character limit, it was not feasible to include SMILES strings, features, and the Nsp15 protein sequence in a single prompt.

Example prompt for GPT models:

"FC(F)(F)CC1CN(CCO1)C(=O)C=C ≫ YES

C=CC(=O)N1CCCCC1C2CCCO2 ≫ NO

Based on the prior examples, for all of the following, predict whether they inhibit or not:

CC1CC=2C=CC=CC2N1C(=O)C=C≫

C=CC(=O)N1CCN(CC1)S(=O)(=O)CC=2C=CON2≫"

Including the Nsp15 protein sequence provided contextual biochemical information potentially enhancing prediction accuracy. For a comprehensive analysis, we engineered prompts that combined chemical structures (SMILES strings) with detailed quantitative features:

"The following are the drug information of molecules that do or do not inhibit the Nsp 15 protein of Covid-19 virus.

Each drug information is presented in one line in the following order: smiles strings, molecular weight, log *P*, number of atoms, number of bonds, number of rings, rotatable bonds count, hydrogen bond donors, hydrogen bond acceptors, number of stereocenters, Topological Polar Surface Area (TPSA).

CNC(=O)CC1CCN(CC1)C(=O)C=C, 210.277, 0.5471, 15, 15, 1, 3, 1, 2, 0, 49.41 ≫ 1

C=CC(=O)N1CCSCC1C#N, 182.248, 0.63998, 12, 12, 1, 1, 0, 3, 1, 44.1 ≫ 0

Based on the prior examples, for all the following, predict whether they inhibit or not. Only output the smiles strings and your predictions, nothing else:

C=CC(=O)NCC(=O)N1CCC=2C=CC=CC2C1, 244.294, 0.8735, 18, 19, 2, 3, 1, 2, 0, 49.41≫

CN(CC(=O)N1CCCC1)C(=O)C=C, 196.25, 0.2532, 14, 14, 1, 3, 0, 2, 0, 40.62≫"

This prompt format provided extensive data for each molecule, allowing the GPT model to generate predictions based on both structural and physical properties.

Performance evaluation metrics. K-Fold cross validation was used to evaluate the performance of models. The value of *k* was considered within 5, 7, and 10. The sampling process 1000 times was considered to prevent data bias, and the average performances were the result. The models were evaluated using various metrics including the area under the ROC curve (AUROC) and the area under the precision–recall curve (AUPR), F1 score, recall and precision. These metrics were calculated from the number of true positives (TP), false positives (FP), true negatives (TN), and false negatives (FN) using the following equations:

$$\text{Recall} = \text{TP/TP} + \text{FN} \quad (1)$$

$$\text{Precision} = \text{TP/TP} + \text{FP} \quad (2)$$

$$\text{F1 score} = 2\ (\text{precision} \times \text{recall})/(\text{precision} + \text{recall}) \quad (3)$$

$$\text{Accuracy} = \text{TP} + \text{TN/TP} + \text{TN} + \text{FP} + \text{FN} \quad (4)$$

The AUC value was considered as the indicator of classification model accuracy. Precision measures the accuracy of positive predictions made by a classifier. Recall, also known as sensitivity or true positive rate, measures the ability of a classifier to correctly identify all positive instances in the dataset. The F1 score is the harmonic mean of precision and recall, providing a single metric that balances both precision and recall.

Conclusions

Inhibition of Nsp15 has the potential to greatly improve the treatment of SCoV-2. Nsp15 is a crucial endoribonuclease present in all coronaviruses that aids viruses in evading the host immune response during viral infection. Nsp15 suppresses the production of interferons by infected cells by cleaving viral RNA. Down-regulating the production of interferons by SCoV-2 infected could have synergistic effects with inhibiting viral replication by preventing neighboring cells from being infected with viruses. Despite its potential, developing inhibitors against Nsp15 has been challenging due to its structural complexity and

large binding interface. HTS against SCoV-2 Nsp15 have yielded a few inhibitors, however these compounds were frequently promiscuous hits or non-potent.

Cysteine reactive acrylamide compounds have had great success as covalent inhibitors of proteins, especially in transforming "undruggable" proteins to druggable. Here, we took this opportunity to screen a never-been-explored acrylamide-based library against Nsp15. Acrylamide-containing drugs show prolonged on-target residence time due to irreversible cysteine engagement. We screened a 2640 acrylamide-based electrophile library and identified ten cysteine reactive inhibitors against Nsp15 with IC_{50}s in the low micromolar range (less than 5 μM). These compounds are non-toxic in mammalian cells. These acrylamide-based inhibitors are specific to Nsp15 and can potentially be utilized as initial hits for targeting other coronaviruses. In conclusion, we present acrylamide-based fragments as new covalent inhibitors of Nsp15 enzymes from various coronaviruses and present a new AI-driven pipeline based on these results for the rapid and cheap identification of future lead compounds.

Data availability

The data and code used in this study are available online at **https://github.com/babakmosavati/AI-Powered-Platform-Drug-Discovery**.

Author contributions

Conceptualization, N. M., D. K. N., B. P. H., R. S., X. D., J. R. U., J. S., M. R. K. M.; methodology, T. B., B. M., L. H. Z., E. M. K., H. W., X. L., S. A. T. D., E. W., S. G., R. N. D., M. S. P., J. S.; software, B. M., T. B., L. H. Z., E. M. K., H. W., X. L., S. A. T. D., M. S. P., E. W.; validation, B. M., T. B., N. M.; formal analysis, B. M., T. B., L. H. Z., E. M. K., H. W., X. L., S. A. T. D., E. W.; investigation, T. B., B. M. and N. M.; resources, N. M., D. K. N., B. P. H., R. S., X. D., J. S.; data curation, N. M. and B. M., T. B.; writing—original draft preparation, T. B., B. M., S. G., N. M.; writing—review and editing, N. M., T. B., B. M., J. S., B. P. H., R. S., X. D., L. H. Z.; visualization, T. B., B. M.; supervision, N. M., J. S.; project administration, N. M.; funding acquisition, N. M., J. S. All authors have read and agreed to the published version of the manuscript.

Conflicts of interest

There are no conflicts to declare.

Acknowledgements

We would like to acknowledge Basil P. Hubbard, Xufang Deng for providing critical suggestions for the manuscript. We would also acknowledge Robert Maxwell from QB3 Mass spectrometry facility for mass spectrometry experiments. The BSL-3 live virus work was supported by the Oklahoma Center for the Advancement of Science and Technology (OCAST) grant HR23096 to Xufang Deng. Niren Murthy would like to acknowledge NIH grants UG3NS115599, R33 and R61DA048444-01, RO1EB029320-01A1, RO1MH125979-01, and funding from the BAKAR Spark award, the Cystic Fibrosis Foundation, and the Innovative Genomics Institute. Julia Schaletzky, and Eddie Wehri were supported by the Henry Wheeler Center for Emerging and Neglected Diseases and through Fastgrants. Robin Stanley would like to acknowledge the in part support by the Intramural Research Program of the NIH, National Institute of Environmental Health Sciences (1ZIAES103340).

References

1 Y. Zhu, J. Li and Z. Pang, *Asian J. Pharm. Sci.*, 2021, **16**, 4–23.
2 C. Pozzi, A. Vanet, V. Francesconi, L. Tagliazucchi, G. Tassone, A. Venturelli, F. Spyrakis, M. Mazzorana, M. P. Costi and M. Tonelli, *J. Med. Chem.*, 2023, **66**, 3664–3702.
3 I. Pauly, A. Kumar Singh, A. Kumar, Y. Singh, S. Thareja, M. A. Kamal, A. Verma and P. Kumar, *Curr. Pharm. Des.*, 2022, **28**, 3677–3705.
4 S. M. R. Hashemian, A. Sheida, M. Taghizadieh, M. Y. Memar, M. R. Hamblin, H. Bannazadeh Baghi, J. Sadri Nahand, Z. Asemi and H. Mirzaei, *Biomed. Pharmacother.*, 2023, **162**, 114367.
5 J. Liu, X. Pan, S. Zhang, M. Li, K. Ma, C. Fan, Y. Lv, X. Guan, Y. Yang and X. Ye, *Lancet Reg. Health West. Pac.*, 2023, **33**, 100694.
6 Y. Duan, H. Zhou, X. Liu, S. Iketani, M. Lin, X. Zhang, Q. Bian, H. Wang, H. Sun, S. J. Hong, B. Culbertson, H. Mohri, M. I. Luck, Y. Zhu, X. Liu, Y. Lu, X. Yang, K. Yang, Y. Sabo, A. Chavez, S. P. Goff, Z. Rao, D. D. Ho and H. Yang, *Nature*, 2023, **622**, 376–382.
7 S. A. Moghadasi, E. Heilmann, A. M. Khalil, C. Nnabuife, F. L. Kearns, C. Ye, S. N. Moraes, F. Costacurta, M. A. Esler, H. Aihara, D. von Laer, L. Martinez-Sobrido, T. Palzkill, R. E. Amaro and R. S. Harris, *Sci. Adv.*, 2023, **9**, eade8778.
8 X. Deng, M. Hackbart, R. C. Mettelman, A. O'Brien, A. M. Mielech, G. Yi, C. C. Kao and S. C. Baker, *Proc. Natl. Acad. Sci. U. S. A.*, 2017, **114**, E4251–E4260.
9 E. Kindler, C. Gil-Cruz, J. Spanier, Y. Li, J. Wilhelm, H. H. Rabouw, R. Zust, M. Hwang, P. V'Kovski, H. Stalder, S. Marti, M. Habjan, L. Cervantes-Barragan, R. Elliot, N. Karl, C. Gaughan, F. J. van Kuppeveld, R. H. Silverman, M. Keller, B. Ludewig, C. C. Bergmann, J. Ziebuhr, S. R. Weiss, U. Kalinke and V. Thiel, *PLoS Pathog.*, 2017, **13**, e1006195.
10 D. Zhang, L. Ji, X. Chen, Y. He, Y. Sun, L. Ji, T. Zhang, Q. Shen, X. Wang, Y. Wang, S. Yang, W. Zhang and C. Zhou, *iScience*, 2023, **26**, 107705.
11 C. K. Yuen, J. Y. Lam, W. M. Wong, L. F. Mak, X. Wang, H. Chu, J. P. Cai, D. Y. Jin, K. K. To, J. F. Chan, K. Y. Yuen and K. H. Kok, *Emerging Microbes Infect.*, 2020, **9**, 1418–1428.
12 C. J. Otter, N. Bracci, N. A. Parenti, C. Ye, L. H. Tan, A. Asthana, J. J. Pfannenstiel, N. Jackson, A. R. Fehr, R. H. Silverman, N. A. Cohen, L. Martinez-Sobrido and S. R. Weiss, *bioRxiv*, 2023, preprint, DOI: **10.1101/2023.11.15.566945**.

13 M. C. Pillon, M. N. Frazier, L. B. Dillard, J. G. Williams, S. Kocaman, J. M. Krahn, L. Perera, C. K. Hayne, J. Gordon, Z. D. Stewart, M. Sobhany, L. J. Deterding, A. L. Hsu, V. P. Dandey, M. J. Borgnia and R. E. Stanley, *Nat. Commun.*, 2021, **12**, 636.
14 M. N. Frazier, I. M. Wilson, J. M. Krahn, K. J. Butay, L. B. Dillard, M. J. Borgnia and R. E. Stanley, *Nucleic Acids Res.*, 2022, **50**, 8290–8301.
15 Y. Kim, J. Wower, N. Maltseva, C. Chang, R. Jedrzejczak, M. Wilamowski, S. Kang, V. Nicolaescu, G. Randall, K. Michalska and A. Joachimiak, *Commun. Biol.*, 2021, **4**, 193.
16 J. Chen, R. A. Farraj, D. Limonta, S. A. Tabatabaei Dakhili, E. M. Kerek, A. Bhattacharya, F. M. Reformat, O. M. Mabrouk, B. Brigant, T. A. Pfeifer, M. T. McDermott, J. R. Ussher, T. C. Hobman, J. N. M. Glover and B. P. Hubbard, *J. Biol. Chem.*, 2023, **299**, 105341.
17 J. Ortiz-Alcantara, K. Bhardwaj, S. Palaninathan, M. Frieman, R. S. Baric and C. C. Kao, *Virus Adapt. Treat.*, 2010, **2**, 125–133.
18 F. Sutanto, M. Konstantinidou and A. Dömling, *RSC Med. Chem.*, 2020, **11**, 876–884.
19 P. Ábrányi-Balogh, L. Petri, T. Imre, P. Szijj, A. Scarpino, M. Hrast, A. Mitrović, U. P. Fonovič, K. Németh, H. Barreteau, D. I. Roper, K. Horváti, G. G. Ferenczy, J. Kos, J. Ilaš, S. Gobec and G. M. Keserű, *Eur. J. Med. Chem.*, 2018, **160**, 94–107.
20 A. O. Walter, R. T. T. Sjin, H. J. Haringsma, K. Ohashi, J. Sun, K. Lee, A. Dubrovskiy, M. Labenski, Z. Zhu and Z. Wang, *Cancer Discovery*, 2013, **3**, 1404–1415.
21 M. S. Davids and J. R. Brown, *Future Oncol.*, 2014, **10**, 957–967.
22 B. A. Lanman, J. R. Allen, J. G. Allen, A. K. Amegadzie, K. S. Ashton, S. K. Booker, J. J. Chen, N. Chen, M. J. Frohn and G. Goodman, *J. Med. Chem.*, 2019, **63**, 52–65.
23 L. Boike, N. J. Henning and D. K. Nomura, *Nat. Rev. Drug Discovery*, 2022, **21**, 881–898.
24 S. Wang, Y. Tian, M. Wang, M. Wang, G. B. Sun and X. B. Sun, *Front. Pharmacol*, 2018, **9**, 353.
25 K. Bhardwaj, J. Sun, A. Holzenburg, L. A. Guarino and C. C. Kao, *J. Mol. Biol.*, 2006, **361**, 243–256.
26 R. Choi, M. Zhou, R. Shek, J. W. Wilson, L. Tillery, J. K. Craig, I. A. Salukhe, S. E. Hickson, N. Kumar, R. M. James, G. W. Buchko, R. Wu, S. Huff, T. T. Nguyen, B. L. Hurst, S. Cherry, L. K. Barrett, J. L. Hyde and W. C. Van Voorhis, *PLoS One*, 2021, **16**, e0250019.
27 S. G. Kathman and A. V. Statsyuk, *MedChemComm*, 2016, **7**, 576–585.
28 E. Resnick, A. Bradley, J. Gan, A. Douangamath, T. Krojer, R. Sethi, P. P. Geurink, A. Aimon, G. Amitai, D. Bellini, J. Bennett, M. Fairhead, O. Fedorov, R. Gabizon, J. Gan, J. Guo, A. Plotnikov, N. Reznik, G. F. Ruda, L. Díaz-Sáez, V. M. Straub, T. Szommer, S. Velupillai, D. Zaidman, Y. Zhang, A. R. Coker, C. G. Dowson, H. M. Barr, C. Wang, K. V. M. Huber, P. E. Brennan, H. Ovaa, F. von Delft and N. London, *J. Am. Chem. Soc.*, 2019, **141**, 8951–8968.
29 S. Parasuraman, *J. Pharmacol. Pharmacother.*, 2011, **2**, 74–79.
30 R. C. Borra, M. A. Lotufo, S. M. Gagioti, M. Barros Fde and P. M. Andrade, *Braz. Oral Res.*, 2009, **23**, 255–262.
31 A. Reichel and P. Lienau, *Handb. Exp. Pharmacol.*, 2016, **232**, 235–260.
32 A. Daina, O. Michielin and V. Zoete, *Sci. Rep.*, 2017, **7**, 42717.
33 B. Bakchi, A. D. Krishna, E. Sreecharan, V. B. J. Ganesh, M. Niharika, S. Maharshi, S. B. Puttagunta, D. K. Sigalapalli, R. R. Bhandare and A. B. Shaik, *J. Mol. Struct.*, 2022, **1259**, 132712.
34 S. B. Bunally, C. N. Luscombe and R. J. Young, *SLAS Discovery*, 2019, **24**, 791–801.
35 A. T. Garcia-Sosa, U. Maran and C. Hetenyi, *Curr. Med. Chem.*, 2012, **19**, 1646–1662.
36 D. F. Veber, S. R. Johnson, H.-Y. Cheng, B. R. Smith, K. W. Ward and K. D. Kopple, *J. Med. Chem.*, 2002, **45**, 2615–2623.
37 A. Daina and V. Zoete, *ChemMedChem*, 2016, **11**, 1117–1121.
38 F. Protti Í, D. R. Rodrigues, S. K. Fonseca, R. J. Alves, R. B. de Oliveira and V. G. Maltarollo, *ChemMedChem*, 2021, **16**, 1446–1456.
39 C. A. Lipinski, F. Lombardo, B. W. Dominy and P. J. Feeney, *Adv. Drug Delivery Rev.*, 2001, **46**, 3–26.
40 Y. C. Martin, *J. Med. Chem.*, 2005, **48**, 3164–3170.
41 G. Xiong, Z. Wu, J. Yi, L. Fu, Z. Yang, C. Hsieh, M. Yin, X. Zeng, C. Wu, A. Lu, X. Chen, T. Hou and D. Cao, *Nucleic Acids Res.*, 2021, **49**, W5–w14.
42 J. Chen, R. Abou Farraj, D. Limonta, S. A. T. Dakhili, E. M. Kerek, A. Bhattacharya, F. M. Reformat, O. M. Mabrouk, B. Brigant and T. A. Pfeifer, *J. Biol. Chem.*, 2023, **299**(11), 105341.
43 E. Şahin, A. Karanfil, M. Çol Ayvaz and E. Şahin, *J. Mol. Struct.*, 2021, **1248**, 131357.
44 B. Van Loy, A. Stevaert and L. Naesens, *Antiviral Res.*, 2024, **228**, 105921.
45 J. Han, B. P. Hubbard, J. Lee, C. Montagna, H. W. Lee, D. A. Sinclair and Y. Suh, *Cell Cycle*, 2013, **12**, 263–270.
46 D. Y. Chen, J. Turcinovic, S. Feng, D. J. Kenney, C. V. Chin, M. C. Choudhary, H. L. Conway, M. Semaan, B. J. Close, A. H. Tavares, S. Seitz, N. Khan, S. Kapell, N. A. Crossland, J. Z. Li, F. Douam, S. C. Baker, J. H. Connor and M. Saeed, *iScience*, 2023, **26**, 106634.
47 Y. Hu, E. M. Lewandowski, H. Tan, X. Zhang, R. T. Morgan, X. Zhang, L. M. C. Jacobs, S. G. Butler, M. V. Gongora, J. Choy, X. Deng, Y. Chen and J. Wang, *ACS Cent. Sci.*, 2023, **9**, 1658–1669.
48 T. Xu, J. D. Venable, S. K. Park, D. Cociorva, B. Lu, L. Liao, J. Wohlschlegel, J. Hewel and J. Yates, *Mol. Cell. Proteomics*, 2006, **5**, S174.
49 T. Xu, S. K. Park, J. D. Venable, J. A. Wohlschlegel, J. K. Diedrich, D. Cociorva, B. Lu, L. Liao, J. Hewel, X. Han, C. C. L. Wong, B. Fonslow, C. Delahunty, Y. Gao, H. Shah and J. R. Yates 3rd, *J. Proteomics*, 2015, **129**, 16–24.
50 D. L. Tabb, W. H. McDonald and J. R. Yates, *J. Proteome Res.*, 2002, 21–26.
51 D. L. Tabb, W. H. McDonald and J. R. Yates 3rd, *J. Proteome Res.*, 2002, **1**, 21–26.

52 S. K. Park, J. D. Venable, T. Xu and J. R. Yates, *Nat. Methods*, 2008, **5**, 319–322.
53 S. K. R. Park, A. Aslanian, D. B. McClatchy, X. Han, H. Shah, M. Singh, N. Rauniyar, J. J. Moresco, A. F. M. Pinto, J. K. Diedrich, C. Delahunty and J. R. Yates III, *Bioinformatics*, 2014, **30**, 2208–2209.
54 C. R. Søndergaard, M. H. Olsson, M. Rostkowski and J. H. Jensen, *J. Chem. Theory Comput.*, 2011, **7**, 2284–2295.
55 K. Roos, C. Wu, W. Damm, M. Reboul, J. M. Stevenson, C. Lu, M. K. Dahlgren, S. Mondal, W. Chen, L. Wang, R. Abel, R. A. Friesner and E. D. Harder, *J. Chem. Theory Comput.*, 2019, **15**, 1863–1874.
56 E. C. Meng, T. D. Goddard, E. F. Pettersen, G. S. Couch, Z. J. Pearson, J. H. Morris and T. E. Ferrin, *Protein Sci.*, 2023, **32**, e4792.
57 E. F. Pettersen, T. D. Goddard, C. C. Huang, E. C. Meng, G. S. Couch, T. I. Croll, J. H. Morris and T. E. Ferrin, *Protein Sci.*, 2021, **30**, 70–82.
58 T. R. Lane, F. Urbina, X. Zhang, M. Fye, J. Gerlach, S. H. Wright and S. Ekins, *Mol. Pharm.*, 2022, **19**, 4320–4332.
59 G. Tu, T. Fu, G. Zheng, B. Xu, R. Gou, D. Luo, P. Wang and W. Xue, *J. Chem. Inf. Model.*, 2024, **64**, 1433–1455.
60 B. Dudas and M. A. Miteva, *Trends Pharmacol. Sci.*, 2024, **45**, 39–55.
61 F. Wong, E. J. Zheng, J. A. Valeri, N. M. Donghia, M. N. Anahtar, S. Omori, A. Li, A. Cubillos-Ruiz, A. Krishnan, W. Jin, A. L. Manson, J. Friedrichs, R. Helbig, B. Hajian, D. K. Fiejtek, F. F. Wagner, H. H. Soutter, A. M. Earl, J. M. Stokes, L. D. Renner and J. J. Collins, *Nature*, 2024, **626**, 177–185.
62 J. P. Vert, *Nat. Biotechnol.*, 2023, **41**, 750–751.
63 G. Turon, J. Hlozek, J. G. Woodland, A. Kumar, K. Chibale and M. Duran-Frigola, *Nat. Commun.*, 2023, **14**, 5736.
64 F. Grisoni, *Curr. Opin. Struct. Biol.*, 2023, **79**, 102527.
65 A. Tropsha, O. Isayev, A. Varnek, G. Schneider and A. Cherkasov, *Nat. Rev. Drug Discovery*, 2024, **23**, 141–155.
66 M. Ballarotto, S. Willems, T. Stiller, F. Nawa, J. A. Marschner, F. Grisoni and D. Merk, *J. Med. Chem.*, 2023, **66**, 8170–8177.
67 J. Jumper, R. Evans, A. Pritzel, T. Green, M. Figurnov, O. Ronneberger, K. Tunyasuvunakool, R. Bates, A. Žídek, A. Potapenko, A. Bridgland, C. Meyer, S. A. A. Kohl, A. J. Ballard, A. Cowie, B. Romera-Paredes, S. Nikolov, R. Jain, J. Adler, T. Back, S. Petersen, D. Reiman, E. Clancy, M. Zielinski, M. Steinegger, M. Pacholska, T. Berghammer, S. Bodenstein, D. Silver, O. Vinyals, A. W. Senior, K. Kavukcuoglu, P. Kohli and D. Hassabis, *Nature*, 2021, **596**, 583–589.